

Response of an atomic Bose-Einstein condensate to a rotating elliptical trap

N.G. Parker and C.S. Adams

Department of Physics, University of Durham, South Road, Durham DH1 3LE, United Kingdom

Abstract. We investigate numerically the response of an atomic Bose-Einstein condensate to a weakly-elliptical rotating trap over a large range of rotation frequencies. We analyse the quadrupolar shape oscillation excited by rotation, and discriminate between its stable and unstable regimes. In the latter case, where a vortex lattice forms, we compare with experimental observations and find good agreement. By examining the role of thermal atoms in the process, we infer that the process is temperature-independent, and show how terminating the rotation gives control over the number of vortices in the lattice. We also study the case of critical rotation at the trap frequency, and observe large centre-of-mass oscillations of the condensate.

PACS numbers: 03.75.Lm, 03.75.Kk

1. Introduction

Recent experiments on dilute atomic Bose-Einstein condensates (BECs) have generated vortex lattices by mechanically rotating the system [1, 2, 3], in analogy to the classic rotating bucket experiment in liquid Helium [4]. The smooth magnetic trap confining the condensate, with trap frequency ω_r , is deformed anisotropically and rotated at frequency Ω . Shape oscillations of the condensate are excited, and the quadrupole mode plays a pivotal role in the evolution of the system: for low rotation frequencies, $\Omega < 0.7\omega_r$, a long-lived quadrupole mode has been observed [5], while for higher rotation frequencies $\Omega \sim 0.7\omega_r$, vortex lattice formation has been seen [1, 2, 3]. In the latter case, vortex formation is seeded by a dynamical instability of the quadrupole mode [6, 7, 8]. Experimental results suggest that the crystallisation of the vortices is temperature-independent [9]. Indeed, the full process of lattice formation has been successfully simulated using the zero temperature Gross-Pitaevskii equation [10, 11, 12] (although other studies found it necessary to include damping effects [13, 14]). These results have also indicated that lattice formation is a two-dimensional effect. An experimental aim in this area is to examine the regime of fastly rotating BECs, and probe exotic phenomena such as vortex melting and the bosonic quantum Hall effect [15]. This has led to the experimental investigation of a BEC under critical rotation [16], where the rotation frequency equals the trap frequency, and super-critical rotation [17].

In this work we investigate the intrinsic response of an atomic BEC to rotation in a weakly-elliptical trap using the zero-temperature Gross-Pitaevskii equation. This is performed over a large range of rotation frequencies, allowing us to probe diverse

regimes of condensate dynamics relevant to current BEC experiments. In the regime of sub-critical rotation, a quadrupole shape mode dominates the dynamics. Close to resonance this mode is unstable and vortex lattice formation occurs, in close agreement with experiments. We simulate the role of thermal atoms in the lattice formation, and consider the effect of terminating the rotation. At critical rotation, $\Omega \approx \omega_r$, we show that large centre-of-mass oscillations dominate the dynamics.

At ultra-cold temperature $T \ll T_c$ (where T_c is the BEC transition temperature) and for a large number of condensate atoms, thermal and quantum effects are minimal, and an atomic BEC can be approximated by a mean-field ‘macroscopic wavefunction’ $\psi(\mathbf{r}, t)$. The dynamics of this wavefunction are well-described by the Gross-Pitaevskii equation (GPE) [19],

$$i \frac{\partial \psi(\mathbf{r}, t)}{\partial t} = \left[-\frac{\hbar^2}{2m} \nabla^2 + V_{\text{ext}}(\mathbf{r}, t) + g |\psi(\mathbf{r}, t)|^2 \right] \psi(\mathbf{r}, t), \quad (1)$$

where $V_{\text{ext}}(\mathbf{r}, t)$ is the external confinement and m is the atomic mass. The nonlinear coefficient $g = 4\pi\hbar^2 Na/m$ governs the atomic interactions, where N is the number of atoms and a is the s -wave scattering length. It is useful to consider the hydrodynamic interpretation of the wavefunction $\psi(\mathbf{r}, t) = \sqrt{n(\mathbf{r}, t)} \exp[i\phi(\mathbf{r}, t)]$, where $n(\mathbf{r}, t)$ is the atomic density and $\phi(\mathbf{r}, t)$ is a phase factor, which defines a fluid velocity via $\mathbf{v}(\mathbf{r}, t) = (\hbar/m)\nabla\phi(\mathbf{r}, t)$.

Vortices in BEC are characterised density node and an azimuthal phase slip, quantized to multiples of 2π (to keep ψ single-valued). The lowest energy state of a BEC in a rotating system (above the critical rotation for the onset of vortices) is an ordered triangular lattice of singly-charged vortices [20] (vortices with multiple ‘charge’ are unstable [21]), whereby the system mimics solid-body rotation. However, an energy barrier exists for vortices to enter the condensate and so the transformation process from a vortex-free state to a vortex lattice is non-trivial. Lattices have been formed thermodynamically [14, 22] by condensing a rotating thermal cloud [23]. In [24], the precession of a small laser ‘stirrer’ above a critical velocity generated vortex excitations locally [25] and ultimately a lattice [10]. Other lattice experiments [1, 2, 3] involve the direct rotation of the condensate in an anisotropic trap, which is the case we will study in this paper. In addition we consider a sudden turn on of the trap rotation rather than the adiabatic introduction of the rotating anisotropy [7, 8]. Condensate shape oscillations are excited, and through a dynamical instability of the dominant quadrupole mode [6, 7, 8], the condensate fragments [12]. Provided the two-fold rotational symmetry of the system is allowed to break, a turbulent state of sound waves (density excitations) and vortices is generated. Subsequently, through the interaction of the vortices with the sound field [26], the vortices gradually become ordered into a lattice configuration.

The trap rotation, which occurs in the x - y plane about the z -axis, strongly polarizes the system. Although bending and Kelvin wave excitation of vortex lines do occur [27], the 2D dynamics in the rotating plane dominate, and a 2D description is sufficient to simulate lattice formation [10, 12, 13]. We therefore proceed by solving the computationally-advantageous 2D GPE in the rotating x - y plane.

In the experiments of [1, 2, 8] the trap is approximately elliptical in the rotating plane with the form,

$$V_{\text{ext}}(x, y, t) = \frac{1}{2} m \omega_r^2 [(x^2 + y^2) + \varepsilon (X(t)^2 - Y(t)^2)]. \quad (2)$$

Here the first term represents the static radial harmonic trap with frequency ω_r . In the second term, ε is the ellipticity parameter of the trap (typically $\varepsilon \ll 1$), and the rotating coordinates $X(t)$ and $Y(t)$ are given by,

$$X(t) = x \cos(\Omega t) - y \sin(\Omega t) \quad (3)$$

$$Y(t) = x \sin(\Omega t) + y \cos(\Omega t), \quad (4)$$

where Ω is the trap rotation frequency. Note that in [3] the trap is strongly anharmonic, rather than weakly-elliptical.

Our units of length and time are the healing length $\xi = \hbar/\sqrt{m\mu}$ and (ξ/c) , where $c = \sqrt{\mu/m}$ is the Bogoliubov speed of sound. The chemical potential $\mu = n_0 g$ is the unit of energy, where n_0 is the peak atomic density. Unless stated otherwise, we employ parameters which match the experiment of Madison *et al.* [1]: our trap ellipticity is $\varepsilon = 0.025$, the chemical potential is $\mu = 10\hbar\omega$, the trap frequency is $\omega_r = 0.1(c/\xi)$, and the Thomas-Fermi radius of the condensate is $R_{\text{TF}} = 14\xi$. For such a ^{87}Rb condensate, our units of time and space correspond to $\xi \sim 0.2 \mu\text{m}$ and $(\xi/c) \sim 10^{-4}$ s.

Our initial state is found by propagating the GPE in imaginary time ($t \rightarrow -it$) subject to the initial potential $V_{\text{ext}}(x, y, t = 0)$ while forcing the peak density to unity. Subsequently the system is run in real time. We generally characterise the state of the system in terms of the condensate energy, which is evaluated according to the GPE energy functional,

$$E = \int \left[-\frac{\hbar^2}{2m} |\nabla\psi|^2 + V_{\text{ext}}|\psi|^2 + \frac{g}{2} |\psi|^4 \right] dx dy. \quad (5)$$

Note that we subtract from equation (5) the energy corresponding to the initial state, i.e. energy is measured relative to the ground state.

In section 2 we investigate the quadrupole mode of a condensate in a rotating trap, and discriminate between the stable and unstable regimes. In the latter case, we observe vortex lattice formation, and in section 3 we compare our results with the lattice experiments. Section 4 infers the role of thermal atoms in the lattice formation, and the effect of terminating the rotation is analysed in section 5. The condensate dynamics under critical and super-critical rotation of the trap are studied in section 6. Finally, section 7 presents the conclusions of this work.

2. The Quadrupole Mode

In the rotating frame, and for slow rotations, the stationary solution in an elliptical trap is an elliptical condensate [6, 28], with the size of the ellipticity depending not only on the trap ellipticity ε but also the rotation frequency Ω . Such a state can be reached by adiabatically ramping up the rotation frequency from 0 to the chosen value, Ω [7]. This technique has been implemented experimentally [8]. In our case, however, the rotation is suddenly turned on with frequency Ω and maintained at this value. The condensate is continuously driven out of equilibrium and never reaches a steady elliptical state. Consequently, collective shape excitations are expected to occur.

Classical hydrodynamics predict that, for a non-rotating trapped condensate, the shape oscillations satisfy the dispersion relation $\omega_\ell = \sqrt{\ell}\omega_r$, where ℓ is the angular momentum quantum number [29]. The two-fold symmetry of our system implies that only even angular momentum modes will be excited, and we expect the lowest order

mode to dominate, i.e. the $\ell = 2$ quadrupolar mode with frequency $\omega_Q^0 = \sqrt{2}\omega_r$. When driven resonantly at half this frequency, i.e. at $\Omega = \omega_r/\sqrt{2}$, this mode is predicted to be dynamically unstable [7], leading to vortex lattice formation. Experimental results [1, 2, 3] and simulations of the GPE [10, 11, 12, 13] have verified this instability, and that it occurs over a range of rotation frequencies in the vicinity of ω_Q^0 .

2.1. Stable quadrupole mode

We first consider the case of the stable quadrupolar mode. Figure 1(a)-(b) shows the condensate density and phase throughout a cycle of the quadrupole oscillation for a rotation frequency $\Omega = 0.7\omega_r$. Note that, due to the rotating trap, the two primary axes of the quadrupole continuously rotate over time at the rotation frequency Ω .

The condensate density initially has a circular shape. Over time it becomes elongated (figure 1 (a)(i)) up to some maximum point (figure 1(a)(ii)). The elongation then decreases (figure 1(a)(iii)) and the condensate returns to a circular state (figure 1(a)(iv)). The phase distribution initially, and after one complete cycle, is uniform. As the condensate becomes elongated (figure(b)(i)-(iii)), the phase develops a quadrupolar structure of the form $\phi(x, y) \propto XY$, where X and Y are the rotating coordinates of the ellipse. This corresponds to a flow of fluid towards and away from the trap centre in different quadrants of the ellipse, as indicated by the arrows in figure 1(b)(i)-(iii). Although the condensate *appears* to be rotating, the combined effect of the quadrupole cycle and the rotation of the quadrupole axes ensures that the fluid remains irrotational at all times [5, 28]. When the condensate is highly elongated (figure 1(ii)), the phase structure is dense, i.e. the fluid velocity is high, as required to maintain the irrotational flow.

The condensate energy (figure 1(c)) oscillates sinusoidally at the quadrupole frequency ω_Q between $E = 0$, representing the circular, ground state condensate, and a maximum value $E = E_{\max}$, corresponding to the fully elongated, excited state. This is analogous to a vortex cycling in and out of a condensate driven by a narrow optical stirrer [30], and to the Rabi oscillations of an atom in a light field. Note that

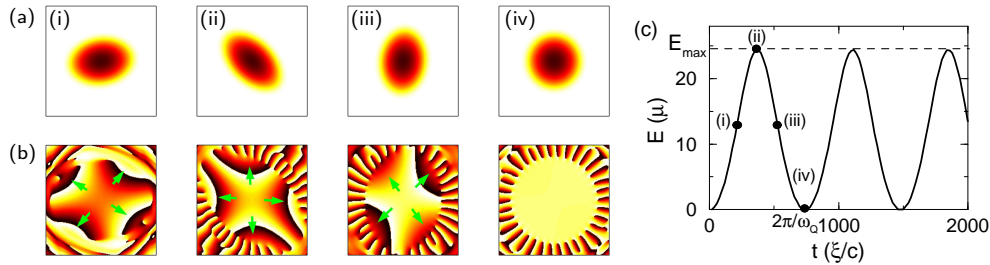


Figure 1. Stable quadrupole mode. (a)-(b) Snapshots in density and phase during one oscillation of quadrupolar flow ($\Omega = 0.7\omega_r$), at times $t =$ (i) 185, (ii) 370, (iii) 555, and (iv) 740 (ξ/c). Each box corresponds to the region $[-25, 25]\xi \times [-25, 25]\xi$. Arrows in (i)-(iii) indicated the direction of fluid flow. Density and phase are shown in the ranges $(0 - n_0)$ and $(-\pi, \pi)$ respectively, with light/dark regions corresponding to low/high values. Note that the complex phase structure at large radii has no meaning since the density is essentially zero. (c) Energy of the condensate during quadrupolar flow. The times of the snapshots in (a)-(b) are indicated.

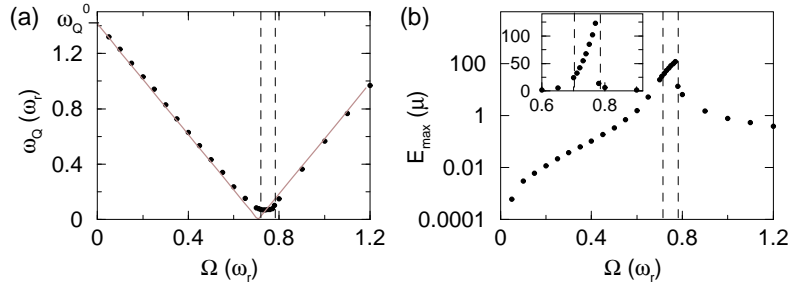


Figure 2. The quadrupole mode. (a) Quadrupole frequency ω_Q as a function of rotation frequency Ω for the numerical data (circles) and the classical hydrodynamic prediction of equation 6 (grey/brown line). (b) Energy amplitude E_{\max} of the quadrupole oscillations as a function of rotation frequency. The y -values are shown on a logarithmic scale. Inset: the central region of the main plot shown with decimal scaling on the y -axis. In all plots the dashed lines indicate the extent of the unstable quadrupole region.

the energy shows no additional behaviour: we do not detect higher order modes (e.g. $\ell = 4, 6, \dots$), and the orientation of the quadrupole (oscillating at Ω) does not affect the energy.

2.2. Behaviour of the quadrupole mode with rotation frequency

The sinusoidal energy evolution in figure 1(c) is a general feature of the quadrupole mode, characterised by the quadrupole frequency ω_Q and amplitude E_{\max} . We now examine the variation of these quantities with rotation frequency Ω . First, consider the quadrupole frequency, shown in figure 2(a). In the limit $\Omega \rightarrow 0$ the quadrupole frequency approaches $\omega_Q^0 \equiv \sqrt{2}\omega_r$, which corresponds to the analytic prediction in a non-rotating system [29]. For a system rotating at frequency Ω the Hamiltonian features an additional centrifugal term $-\Omega L_z$ [20], where L_z is the z -component of the angular momentum. This adds a shift of $-\ell\Omega$ to the dispersion relation. For the quadrupole $\ell = 2$ mode this gives,

$$\omega_Q(\Omega) = |\omega_Q^0 - 2\Omega|. \quad (6)$$

This equation is plotted in figure 1(a) (grey/brown line) and fits the numerical data well for rotation frequencies away from the quadrupole resonance at $\Omega = \omega_Q^0/2$. However, close to this resonance, the data deviates from the linear trend and never reaches zero. This is the unstable region of the quadrupolar mode, which ultimately leads to vortex lattice formation [12]. Note that the unstable regime lies in the vicinity of, but not necessarily centred around, the analytic prediction of $\Omega = \omega_Q^0/2$. This shift is due to the elliptical perturbation on the system. The extent of this unstable region and how it compares to experimentals will be discussed in section 3. The amplitude of the quadrupole mode, shown in figure 2(b), increases towards the region of instability. Close to and within this region, the amplitude becomes extremely large. The unstable quadrupole region is therefore associated with when the quadrupole mode has a frequency close to zero and a large amplitude.

3. Comparison with experimental observations

3.1. Width of the unstable region and number of vortices

In the experiment of Madison *et al.* [1], lattice formation was observed in the region $0.68 \leq \Omega/\omega_r \leq 0.78$. Below this no vortices were observed, while above this the condensate became turbulent. Figure 3(a) shows the final number of vortices we observe in the lattice for different rotation frequencies. To be consistent with the experimental observations, where density imaging has limited accuracy, we only count a vortex if it resides in a region of significant density, which we take to be where the density is greater than $n \approx 0.2n_0$. This also avoids the counting of the phase singularities at very low density which have negligible energy. The range of rotation frequencies over which we observe lattice formation, $0.72 < \Omega/\omega_r < 0.78$, is comparable to the experimental observations. Within this region, we observe the final number of vortices to increase with rotation frequency up to 12 vortices.

Both below *and above* the lattice-forming region we observe stable quadrupolar oscillations, with no indication of a turbulent regime. Note that for super-critical rotations $\Omega/\omega_r > 1$ no more condensate atoms were observed in the experiment. We will consider this regime in section 6.

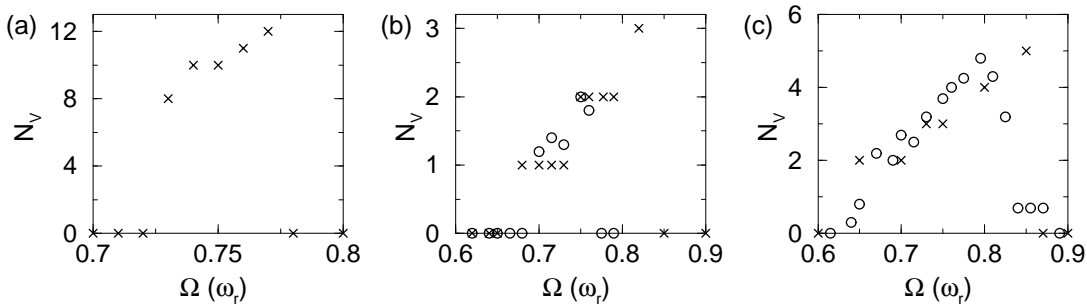


Figure 3. Number of vortices in the final lattice versus rotation frequency for (a) the system of Madison *et al.* [1] with trap ellipticity $\varepsilon = 0.025$, and the system of Hodby *et al.* [2] with trap ellipticities of (b) $\varepsilon = 0.041$ and (c) $\varepsilon = 0.084$. Numerical results are shown by crosses. In (b)-(c) the experimental data (averaged over four observations) from [2] is shown by circles.

We now consider the experiment of Hodby *et al.* [2], and employ a system with chemical potential $\mu \approx 4\hbar\omega_r$ and trap frequency $\omega_r \approx 0.25(c/\xi)$, which has a Thomas-Fermi radius of $R_{\text{TF}} \approx 6\xi$. Figure 3(b)-(c) shows the number of vortices produced as a function of Ω for two different trap ellipticities of (b) $\varepsilon = 0.041$ and (c) $\varepsilon = 0.084$. The experimental observations of Hodby *et al.* [2] are shown by circles, while the numerical results from the GPE are shown by crosses. We see good agreement between theory and experiment, both in the extent of the lattice-forming region and the number of vortices produced, and particularly for the higher value of the ellipticity. By comparing figures 3(b) and (c), we see that the width of the unstable regime and the number of vortices produced increase with trap ellipticity. The number of vortices produced here is lower than for the parameters of Madison *et al.* since the condensate is smaller. Note that Lundh *et al.* [10] have modelled this experiment using the 2D GPE (albeit for different data) and also found good agreement.

3.2. Symmetry breaking and the timescale for lattice formation

In our simulations of the unstable quadrupole regime, numerical noise grows exponentially and ultimately breaks the symmetry on a macroscopic level [12]. In real systems, noise arises from many sources, e.g. thermal/quantum fluctuations, trap imperfections and stray fields, and will have a similar symmetry-breaking effect, albeit on a much larger scale. In order to model such ‘real-life’ effects we impose a random ‘jitter’ on the trap centre, limited to the region $[-\gamma, \gamma] \times [-\gamma, \gamma]$. The parameter γ therefore allows us to control numerically the degree of symmetry-breaking. Conveniently, even a very small jitter, e.g. $\gamma = 0.0001\xi$, is sufficient to dominate over the effects of numerical noise [12]. However, the final state of the lattice, e.g. the number of vortices, is insensitive to γ . We will employ a jitter of $\gamma = 0.1\xi$, which corresponds to around 20 nm.

We return to using the system parameters of Madison *et al.* [1]. Figure 4(a) shows the evolution of the condensate energy for various rotation frequencies within the unstable region. Figure 4(b) shows the corresponding evolution of the elliptical deformation of the condensate α defined as,

$$\alpha = \Omega \frac{\langle X^2 \rangle - \langle Y^2 \rangle}{\langle X^2 \rangle + \langle Y^2 \rangle}, \quad (7)$$

where $\langle X^2 \rangle = \int X^2 |\psi(x, y = 0)|^2 dX$ and $\langle Y^2 \rangle = \int Y^2 |\psi(x = 0, y)|^2 dY$. These curves have the same qualitative features, which are related to the key stages in the evolution [12].

Fragmentation: The quadrupole mode becomes over-excited and atoms are ejected.

Partial quadrupole oscillations occur (where the condensate does not fully return to its circular state), with the energy undergoing partial oscillations.

Symmetry breaking and turbulence: When the system asymmetry has grown to macroscopic levels the quadrupole oscillations cease. Energy is rapidly coupled into the condensate up to some maximum value. At this point the condensate is a turbulent state of vortices and sound waves. Note it also returns to having an approximately circular shape.

Crystallisation: The total energy stays approximately constant, while vortex-sound interactions allow the vortices to settle into a lattice configuration.

As apparent in figure 4, the length of the fragmentation stage is highly sensitive to the trap rotation frequency. In the shortest case (solid black line in figure 4), the fragmentation stage persists for a time of around $3000(\xi/c)$ (or 300 ms). On the other hand, the timescale for the symmetry-breaking/turbulent stage is insensitive to these effects, and typically extends for a time of around $1000(\xi/c)$ (or 100 ms). The crystallisation phase in our simulations is also independent of these effects and remains a slow process, typically taking $50000 - 10000 (\xi/c)$ (or $0.5 - 1$ s) to form a well-ordered lattice.

In the experiments [1, 2, 8], the condensate is observed to undergo partial quadrupole oscillations (where the condensate does not fully return to a circular state), become disordered, and finally form an ordered vortex lattice. This appears to be consistent with the stages of lattice formation described above. Indeed, in [8] the elliptical deformation of the condensate is measured as a function of time, and bears the same qualitative features as in figure 4(b).

We now compare our simulations to the experimentally-observed timescales, where possible. In [8], the partial shape oscillations occur for approximately 250 ms.

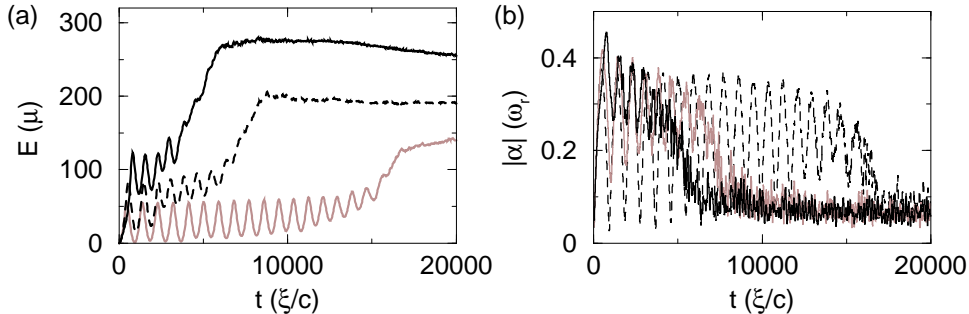


Figure 4. (a) Evolution of the condensate energy for rotation frequencies 0.73 (solid grey/brown line), 0.75 (dashed black line) and 0.77 (solid black line). (b) Evolution of the elliptical deformation of the condensate, defined by equation (7), for the corresponding cases. A trap jitter of $\gamma = 0.1\xi$ is employed. Note that the time unit corresponds to $(\xi/c) \sim 10^{-4}$ s.

Subsequently, the experimental shape oscillations cease and the condensate returns to an approximately circular shape. This occurs over a time of around 50 ms. These timescales are comparable with the quickest evolution in figure 4 (solid lines).

In the experiments, a lattice is observed after $(0.5 - 1)$ s of trap rotation, where in our simulations [12] it takes the equivalent of approximately 10 seconds for the lattice to become well-ordered. We have shown that the timescale for the fragmentation, symmetry-breaking and turbulent phases are consistent with experimental observations, and so this time anomaly must lie with the crystallisation phase. This discrepancy in the crystallisation rate may be due to thermal dissipation (although results in section 4 would contradict this) or 3D effects such as Kelvin wave excitation and damping [27], both of which are not present in our simulations.

4. The role of ‘thermal’ atoms

In the classical field interpretation [18], the GPE describes both the mean-field condensate *and* the fluctuating thermal field of random excitations. The thermal excitations typically have high energy and momenta in comparison to the condensate. As described in [12], an integral part of the lattice formation process is the irreversible generation of a highly-energetic outer cloud, which we will interpret as thermal atoms.

The numerical grid on which the simulations are performed naturally imposes a momentum cutoff into the system. In our square 2D system, with isotropic grid spacing δ , the k -values are restricted to a square region $|k_{x,y}| \leq k_{\max}$, where $k_{\max} = 2\pi/\delta$. We employ an isotropic grid spacing $\delta = 0.25\xi$, which is sufficiently small that it does not restrict directly the dynamics of the condensate. However, it will affect the thermal component of the system. High energy atoms will ‘evaporate’ from the system when they exceed this cutoff. For example, consider the total energy and norm during the lattice formation process (figure 5, solid black lines). The total norm does not visibly decrease, yet a very small proportion of thermal atoms are lost. These are the most energetic atoms, causing a gradual decrease in the energy at later times (figure 5(a), solid black line).

We investigate the role of the classical thermal cloud in the lattice formation

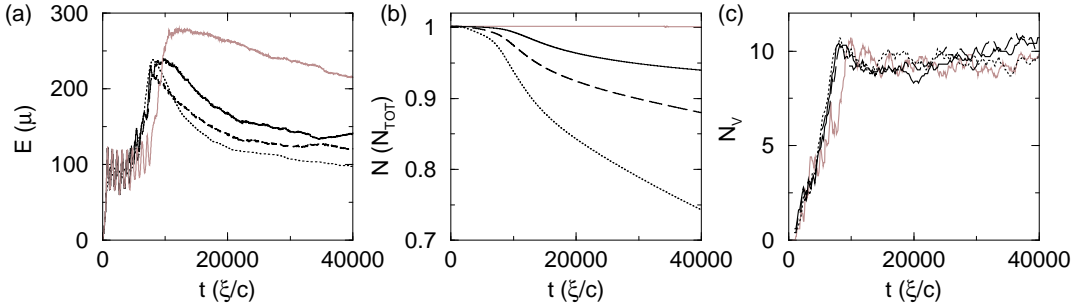


Figure 5. Effect of momentum cutoff on lattice formation. (a) Evolution of the condensate energy for the unimposed case (grey/brown line), where the allowable k -values are restricted by the numerical grid to a *square* region $[k_x, k_y \leq k_{\text{max}}]$, and imposed *circular* regions with radius $k_{\text{cut}} = k_{\text{max}}$ (solid black line), $0.8k_{\text{max}}$ (dashed black line), and $0.6k_{\text{max}}$ (dotted black line). Here $k_{\text{max}} = 2\pi/\delta$ is the maximum allowable k -value, which is set by the isotropic grid size δ . (b) The norm of the condensate for the same cases. (c) Number of vortices in the condensate for these four cases.

process by varying the cutoff in k -space. To impose a cutoff at k_{cut} , we Fourier transform into k -space, set $|\psi(k_x, k_y)| = 0$ for values which satisfy $(k_x^2 + k_y^2)^{1/2} > k_{\text{cut}}$, and then inverse Fourier transform to obtain the modified spatial wavefunction. This is repeated regularly throughout the simulation (every 100 time steps). Note that the imposed cutoff is circular in k -space, in contrast to the square cutoff induced by the grid.

Figure 5 also shows the dynamics for various imposed circular cutoffs: $k_{\text{cut}} = k_{\text{max}}$ (grey/brown solid line), $0.8k_{\text{max}}$ (grey/brown dashed line), and $0.6k_{\text{max}}$ (grey/brown dotted line). These cases exhibit some common features. Despite the reduction in the population of thermal atoms, a vortex lattice forms in all cases. Importantly, the lattices contains approximately the same number of vortices (figure 5(c)). The peak condensate energy (figure 5(a)) is slightly lower than the case of no imposed cutoff (black line). In the crystallisation phase the energy decreases exponentially, and at a faster rate than the case of no imposed cutoff. Similarly, for the norm (figure 5(b)), atoms are lost during the lattice formation process, and the rate of loss increases as the cutoff is reduced. These features are to be expected since lowering the cutoff ‘evaporates’ more energetic atoms from the system. However, the number of vortices in the condensate does not visibly decrease, indicating that this energy/particle loss has little or no affect on the vortex dynamics in the central condensate.

What is somewhat surprising is the significant difference in the energy curves between the square cutoff (figure 5(a), black solid line) and the circular cutoff with the same width (figure 5(a), grey/brown solid line). Clearly a large amount of energy must accumulate in the high- k corners of k -space.

For the imposed cutoffs, the energy has very similar dynamics, despite the large variations in the cutoff. In particular, the exponential decay of the energy during the crystallisation stage occurs on similar timescales. Furthermore, the number of vortices in the final lattice is insensitive to the cutoff. This suggests that the formation of the lattice is independent of the number of thermal atoms, and therefore independent

of temperature. Experimental evidence to suggest that the crystallisation stage is temperature-independent has been presented in [2, 9].

5. Effect of terminating the rotation

So far we have considered a condensate in a trap which is under *continuous* rotation. Here we study the effect of terminating the rotation after some time. We first consider the case of the stable quadrupole mode (described in section 2). This cycle is driven and maintained by the continuous trap rotation. Terminating the rotation freezes the energy and elongation of the condensate. The quadrupole mode ceases although the elongated condensate still rotates at the rotation frequency.

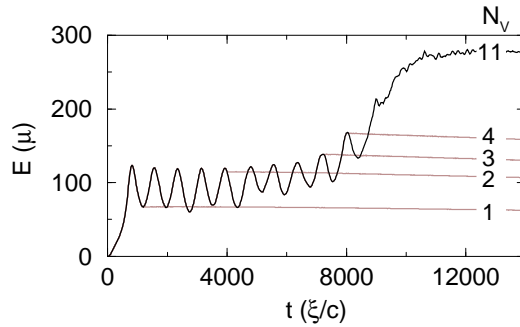


Figure 6. Effect of terminating the rotation. Evolution of the condensate energy for continuous rotation (black line), and rotation which is terminated at times $t =$ (i) 1180, (ii) 4000, (iii) 7200, and (iv) 8000 (ξ/c). The number of vortices produced in each case is indicated.

Figure 6 presents results for the unstable quadrupole regime. Here the energy for the case of continuous rotation (black line) is compared with cases where the rotation is turned off at various times (grey/brown lines). Once the rotation is terminated, no more energy can be coupled into the system, and the total energy becomes approximately fixed (some energy is lost due to the finite momentum cutoff - see section 4). In all cases shown a vortex lattice is ultimately produced, including the case where the rotation is terminated after just one quadrupole oscillation. This implies that once the instability has been started, i.e. the fragmentation during the first quadrupole oscillation, the full vortex formation process will occur.

An interesting effect of terminating the rotation is that, because the energy of the system becomes fixed, it allows control over the number of vortices in the final lattice. For example, under continuous rotation the final state in figure 6 (black line) contains a maximum value of 11 vortices. However, for the cases where the rotation is terminated (grey/brown lines) the final state contains 1, 2, 3 and 4 vortices. In principle using this technique it should be possible to generate final lattices containing any number of vortices up to the maximum value.

6. Critical rotation

The fast rotation of condensates at the critical frequency $\Omega = \omega_r$ and above is of current interest, with the prospect of ultimately generating exotic phenomena such as

vortex melting and a quantum Hall state of bosons [15]. For a gas of classical non-interacting particles under critical rotation the centrifugal force equals the trapping force, and the particles are no longer confined [31]. Super-critical rotation has been studied experimentally in a harmonic trap featuring an additional quartic term to avoid this singularity [17]. Rosenbusch *et al.* [16] investigated critical rotation in a rotating trap both experimentally and theoretically, and showed that, while the non-interacting (non-condensed) gas explodes, repulsive interactions can hold the condensate together. This occurs if the trap ellipticity does not exceed a critical value (of the order of $\varepsilon \sim 0.1$). Then the centre of mass of the condensate is destabilised and spirals away from the trap centre. However, if ε exceeds the critical value, the condensate also undergoes explosive dynamics. Note that the values of ellipticity used throughout this paper are well within this critical ellipticity.

We now consider the response of our system to critical and super-critical trap rotation. As shown in figure 2, there is no strange behaviour in the quadrupole mode as the critical point is reached and exceeded - the frequency/amplitude continue to increase/decrease in a smooth manner. However, we do observe additional dynamics under critical rotation, namely the periodic spiralling of the condensate in and out of the trap centre. This is in partial agreement with Rosenbusch *et al.* [16], who conclude that spiralling condensate does not return to the centre of the trap. As with lattice formation, these dynamics require the initial two-fold symmetry of the system must be broken. Although this will occur slowly due to numerical noise, we impose a trap jitter to speed up the dynamics, unless stated otherwise. Figure 7(a)(solid line) shows the evolution of the condensate energy for critical rotation $\Omega = \omega_r$. The energy undergoes huge oscillations. This corresponds to the periodic centre-of-mass motion of the condensate to large radii in the trap (figure 7(b)). Quadrupolar shape oscillations of the condensate still occur, but the energy amplitude of the quadrupole oscillations (see figure 2(b)) is three orders of magnitude smaller than these oscillations. In the absence of an imposed trap jitter (dotted line in figure 7(a)), the centre-of-mass

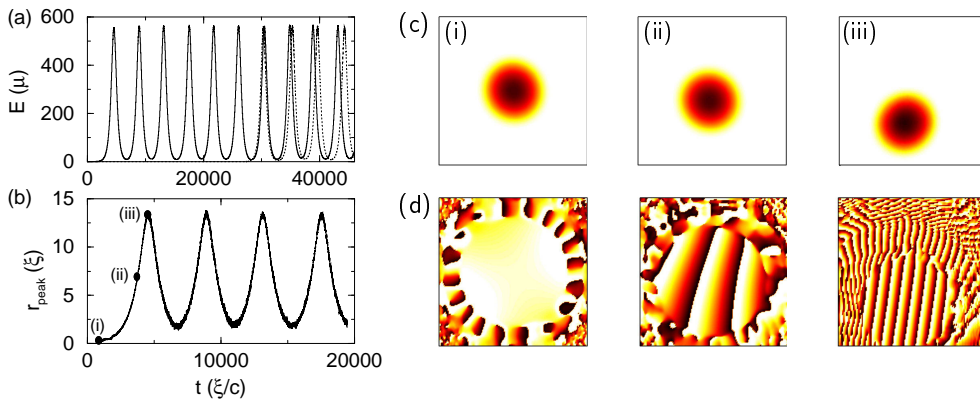


Figure 7. Critical rotation. (a) Evolution of the total condensate energy for critical rotation $\Omega = \omega_r$ with trap jitter $\gamma = 0.1$ (solid line), and with no trap jitter (dotted line). (b) Radius of the condensate peak (with trap jitter). (c) Density and (d) phase plots of the condensate during the centre-of-mass precession at times $t =$ (i) 500, (ii) 3500, and (iii) 4500 (ξ/c). These times are indicated in (b).

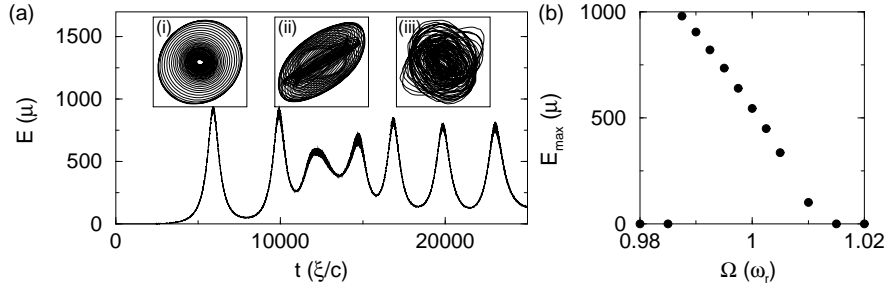


Figure 8. Rotation at $\Omega = 0.99\omega_r$. (a) Condensate energy for a rotation frequency $\Omega = 0.99\omega_r$ (with trap jitter $\gamma = 0.1\xi$). Insets show the path of the condensate peak during the times (i) 3000 – 6000, (ii) 9000 – 12000, and (iii) 18000 – 23000 (ξ/c). (b) Initial energy amplitude E_{\max} of the centre-of-mass motion.

dynamics begin after the system has evolved for some time at low energies.

Figure 7(b)-(c) shows the density and phase during the centre-of-mass oscillations. The condensate begins with approximately circular shape and uniform phase (snapshot (i) in figure 7(c)-(d)). It slowly drifts away from the trap centre (figure 7(c), snapshot (ii)) while precessing quickly at the rotation frequency. A striking quasi-linear phase structure develops (figure 7(d), snapshot (ii)), which represents the bulk motion of the condensate in the tangential direction. At a later time (figure 7(c)-(d), snapshot (iii)), the condensate is further from the trap centre, and here the linear phase structure is more concentrated. Periodically the condensate returns back to the trap centre.

We observe that this centre-of-mass motion occurs in a range of frequencies around the critical frequency. However, the centre-of-mass precession is not always of constant amplitude and frequency. Figure 8(a) shows the condensate dynamics for a rotation frequency of $\Omega = 0.99\omega_r$. Here the energy oscillates with varying frequency and amplitude. As shown in the insets of figure 8(a), this is due to the condensate moving in an ellipse, rather than a circle, with the ellipticity and axes of the ellipse clearly changing with time.

We characterise the size of the centre-of-mass motion in terms of the amplitude of the initial energy oscillations. Figure 8(b) shows this energy amplitude E_{\max} for rotation frequencies around the critical point. We clearly see that the centre-of-mass motion occurs in the narrow frequency range $0.985 < \Omega/\omega_r < 1.015$. In [16] this range is predicted to be $\sqrt{1-\varepsilon} < \Omega/\omega_r < \sqrt{1+\varepsilon}$, giving $0.987 < \Omega/\omega_r < 1.012$, which is in good agreement with our observations. The irregular centre-of-mass motion occurs in the lower part of this range, for $\Omega/\omega_r < 0.9975$, where the condensate is excited to the highest energies.

Above this critical region, the centre-of-mass oscillations cease and the dominant excitation in the condensate returns to being the quadrupole mode, albeit with very low amplitude (see figure 2).

We have also considered the critical rotation of a condensate which contains vortices, both by forming a vortex lattice at $\Omega \sim 0.7\omega_r$ and suddenly switching the rotation to $\Omega = \omega_r$, and by slowly ramping the rotation, through the unstable regime, up to $\Omega = \omega_r$. In both cases, we observe the condensate to undergo centre-of-mass oscillations in the trap. However, here the oscillating condensate typically has a diffuse

and disordered appearance, and contains several vortices.

7. Conclusions

In this paper, we have investigated the dynamics of an atomic Bose-Einstein condensate in a weakly-elliptical rotating trap using the two-dimensional Gross-Pitaevskii equation. This was performed over a wide range of rotation frequencies relevant to current experiments. The quadrupole mode of the condensate plays a key role in the dynamics, with the fate of the system depending crucially on the rotation frequency. We resolve the stable and unstable regimes of the quadrupole oscillations. The unstable regime occurs around the resonant frequency of the quadrupole mode, $\omega_Q^0 = \omega_r/\sqrt{2}$, and rotation within this range ultimately leads to vortex lattice formation. Indeed, over the large range of rotations investigated here, we only observe vortex nucleation to occur within this range, i.e. vortex nucleation in elliptical traps only occurs through the dynamical instability of the quadrupole mode. We compare with lattice experiments and find good qualitative, and sometimes quantitative, agreement, despite the limitations of the model we employ (two-dimensional and zero-temperature). This reinforces the idea that lattice formation is at heart a two-dimensional effect. Furthermore, we find that the process is insensitive to the cutoff of ‘thermal’ atoms in the system, suggesting that lattice formation is a zero-temperature phenomenon.

By terminating the trap rotation during the lattice formation process we show that it is possible to control the number of vortices in the final lattice. Finally, we considered the response of the system to critical rotation at the trap frequency, and observe large centre-of-mass oscillations of the condensate, without the explosive dynamics expected for a classical particle.

Acknowledgments

We thank S. A. Gardiner for discussions and C. J. Foot for the use of the experimental data in figure 3. We acknowledge funding from the UK EPSRC.

References

- [1] Madison K W, Chevy F, Wohlleben W and Dalibard J 2000 *Phys. Rev. Lett.* **84** 806
- [2] Hodby E *et al.* 2001 *Phys. Rev. Lett.* **88** 010405
- [3] Abo-Shaeer J R, Raman C, Vogels J M and Ketterle W 2001 *Science* **292** 476
- [4] Osborn D V 1950 *Proc. Phys. Soc. A* **63** 909
- [5] Chevy F, Madison K W and Dalibard J 2000 *Phys. Rev. Lett.* **85** 2223; Hechenblaikner *Get al.* 2002 *Phys. Rev. Lett.* **88** 070406
- [6] Recati A, Zambelli F and Stringari S 2001 *Phys. Rev. Lett.* **86** 377
- [7] Sinha S and Castin Y 2001 *Phys. Rev. Lett.* **87** 190402
- [8] Madison K W, Chevy F, Bretin V and Dalibard J 2001 *Phys. Rev. Lett.* **86** 4443
- [9] Abo-Shaeer J R, Raman C and Ketterle W 2002 *Phys. Rev. Lett.* **88** 070409
- [10] Lundh E, Martikainen J P and Suominen K A 2003 *Phys. Rev. A* **67** 063604
- [11] Lobo C, Sinatra A, and Castin Y 2004 *Phys. Rev. Lett.* **92** 020403
- [12] Parker N G and Adams C S 2005 *Preprint cond-mat/0505730*
- [13] Tsubota M, Kasamatsu K, and Ueda M 2002 *Phys. Rev. A* **65** 023603; Kasamatsu K, Tsubota M and Ueda M 2003 *Phys. Rev. A* **67** 033610
- [14] Penckwitt A A, Ballagh R J and Gardiner C W 2002 *Phys. Rev. Lett.* **89** 260402
- [15] Ho T L 2001 *Phys. Rev. Lett.* **87** 060403; Fetter A L 2001 *Phys. Rev. A* **64** 063608; Cooper N R, Wilkin N K and Gunn J M F 2001 *Phys. Rev. Lett.* **87** 120405

- [16] Rosenbusch P *et al.* 2002 *Phys. Rev. Lett.* **88** 250403
- [17] Bretin V, Stock S, Seurin Y and Dalibard J 2004 *Phys. Rev. Lett.* **92** 050403
- [18] Davis M J, Morgan S A and Burnett K 2001 *Phys. Rev. Lett.* **87** 160402; Goral K, Gajda M and Rzazewski K 2001 *Opt. Express* **8** 92; Norrie A A, Ballagh R J and Gardiner C W 2005 *Phys. Rev. Lett.* **94** 040401
- [19] Dalfovo F, Giorgini S, Pitaevskii L P and Stringari S 1999 *Rev. Mod. Phys.* **71** 463
- [20] A. L. Fetter and A. A. Svidzinsky, *J. Phys. Condens. Matter* **13**, R135 (2001).
- [21] Y. Shin *et al.*, *Phys. Rev. Lett.* **93**, 160406 (2004).
- [22] J. E. Williams *et al.*, *Phys. Rev. Lett.* **88**, 070401 (2002).
- [23] P. C. Haljan, I. Coddington, P. Engels, and E. A. Cornell, *Phys. Rev. Lett.* **87**, 210403 (2001).
- [24] C. Raman *et al.*, *Phys. Rev. Lett.* **87**, 210402 (2001).
- [25] C. Raman *et al.*, *Phys. Rev. Lett.* **83**, 2502 (1999); B. Jackson and J. F. McCann and C. S. Adams, *Phys. Rev. Lett.* **80**, 3903 (1998).
- [26] N. G. Parker, N. P. Proukakis, C. F. Barenghi, and C. S. Adams, *Phys. Rev. Lett.* **92**, 160403 (2004); M. Leadbeater *et al.*, *Phys. Rev. Lett.* **86**, 1410 (2001).
- [27] V. Bretin *et al.*, *Phys. Rev. Lett.* **90**, 100403 (2003); M. Leadbeater, D. C. Samuels, C. F. Barenghi, and C. S. Adams, *Phys. Rev. A* **67**, 015601 (2003); K. Kasamatsu, M. Machida, N. Sasa, and M. Tsubota, *Phys. Rev. A* **71**, 063616 (2005).
- [28] D. L. Feder, C. W. Clark, and B. I. Schneider, *Phys. Rev. A* **61**, 011601 (2000).
- [29] S. Stringari, *Phys. Rev. Lett.* **77**, 2360 (1996).
- [30] B. M. Caradoc-Davies, R. J. Ballagh, and K. Burnett, *Phys. Rev. Lett.* **83**, 895 (1999).
- [31] D. A. Butts and D. S. Rokhsar, *Nature (London)* **397**, 327 (1999).